Trimethylsilyl-Terminated Oligo(phenylene ethynylene)s: An Approach to Single-Molecule Junctions with Covalent Au–C σ-Bonds

ARTICLE *in* JOURNAL OF THE AMERICAN CHEMICAL SOCIETY · NOVEMBER 2012

Impact Factor: 12.11 · DOI: 10.1021/ja307544w · Source: PubMed

8 AUTHORS, INCLUDING:

Wenjing Hong
Xiamen University
37 PUBLICATIONS **1,716** CITATIONS
SEE PROFILE

Veerabhadrarao Kaliginedi
Universität Bern
13 PUBLICATIONS **228** CITATIONS
SEE PROFILE

Silvio Decurtins
Universität Bern
273 PUBLICATIONS **6,359** CITATIONS
SEE PROFILE

JACS
JOURNAL OF THE AMERICAN CHEMICAL SOCIETY
Article
pubs.acs.org/JACS

Trimethylsilyl-Terminated Oligo(phenylene ethynylene)s: An Approach to Single-Molecule Junctions with Covalent Au−C σ-Bonds

Wenjing Hong, Hui Li, Shi-Xia Liu,* Yongchun Fu, Jianfeng Li, Veerabhadrarao Kaliginedi, Silvio Decurtins, and Thomas Wandlowski*

Department of Chemistry and Biochemistry, University of Bern, CH-3012 Bern, Switzerland

Supporting Information

ABSTRACT: A new and efficient approach using cleaving of trimethylsilyl groups to create covalent Au−C anchoring sites has been developed for single-molecule junction conductance measurements. Employing the mechanically controllable break junction (MCBJ) technique in liquid, we demonstrate the formation of highly conducting single molecular junctions of several OPE derivatives. The created junctions are mechanically stable and exhibit conductances around one order of magnitude higher than those of their dithiol analogues. Extended assembly and reaction times lead to oligomerization. Combined STM imaging and gap-mode Raman experiments provide structure evidence to support the formation of covalent Au−C contacts and further oligomerization.

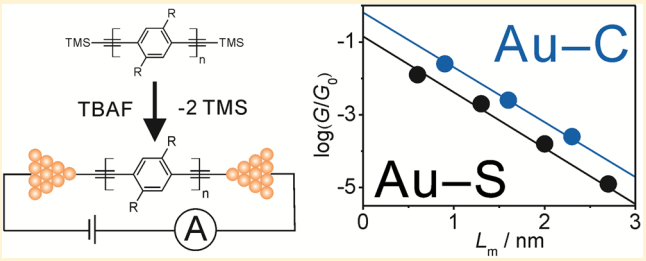

INTRODUCTION

The formation of well-defined, stable, and highly conducting contacts between (single) molecules and electrodes represents a major challenge for charge transport in nanoscale assemblies.[1−5] The most frequently used chemical anchoring groups to bind organic molecules to metal electrodes are thiol (-SH),[1,6,7] amino ($-NH_2$)[8] and pyridyl.[9−11] Other anchoring groups explored are isocyano (-NC),[12,13] cyano (-CN),[14,15] isothiocyanato (-NCS),[16] methylselenide ($-SeCH_3$),[17] methylthiol ($-SCH_3$),[17] fused thiophene,[17] dimethylphosphine,[17] carboxylic acid (-COOH),[6] dithiocarboxylic acid (-CSSH),[18] nitro ($-NO_2$),[15] and even fullerene.[19−22] However, most of these experiments suffer from detriments as non-uniform binding geometries and structural rearrangements of the leads, strong metal−molecule coupling disturbing the molecular orbitals, or decoupled electron systems with limited current flow through the molecular junction.[1,4,7,23,24]

Rather high single-molecule junction conductances were reported for metal−carbon (C) coupling, such as C_{60},[19] benzene,[25] and π-stacked benzene[26] on gold (Au) and platinum (Pt) electrodes. As an important new development, Venkataraman et al. demonstrated recently the formation of direct Au−C-bonded single molecular junctions for alkanes and π-conjugated aromatic molecules upon the spontaneous cleavage of a trimethyl tin end group ($-Sn(CH_3)_3$).[27,28] These covalent σ-bonded junctions led to conductances up to ∼100 times larger compared to analogous alkanes or aromatic molecules with most other terminations. However, the widespread application of this unique approach is currently limited by the need of rather toxic precursors and the immediate formation of dimers and oligomers.[27,28]

Alternative strategies to create covalent, highly directional single metal (e.g., Au, Pt)−C bonds may involve aryldiazonium salts[29−33] or alkynyl compounds.[34−42] Transition metal alkynyl σ-complexes are well-known in the context of organometallic coordination chemistry.[34,35] However, anchoring a molecule via an alkynyl group through a covalent carbon σ-bond to metal surfaces such as gold and other coinage metals,[37,38] remains challenging.

Indeed, several groups reported the grafting of R−C≡CH derivatives on rough[36] and single crystalline Au(111) surfaces,[39,40] as well as on gold nanoparticles.[37,38,41] DFT calculations on the adsorption of an ethynylbenzene radical on Au(111) showed that a strong covalent bond is formed with the surface upon removal of the terminal hydrogen of the ethynyl group.[39] The fcc hollow sites are the most energetically favorable with an interaction energy of ∼2.99 eV per bond. The molecule is proposed to be adsorbed perpendicularly to the surface through the terminal carbon. The authors in ref 39 discuss also an alternative pathway involving the heterolytic cleaving of the C−H bond in R−C≡CH, followed by the surface binding of an anion. This route is thought to be favorable in solution. Transport calculations based on the nonequilibrium Greeńs function (NEG) technique suggests rather high conductances for Au−C≡C−Au single molecular junctions.[42]

Inspired by the above experimental results and theoretical predictions, we applied well-established protecting group chemistry as a novel concept to create single-molecule junctions with covalent Au−C σ-bonds. In this contribution

Received: July 31, 2012
Published: November 5, 2012

   dx.doi.org/10.1021/ja307544w | J. Am. Chem. Soc. 2012, 134, 19425−19431

Scheme 1. Schematics of the Au−C Junction Formation

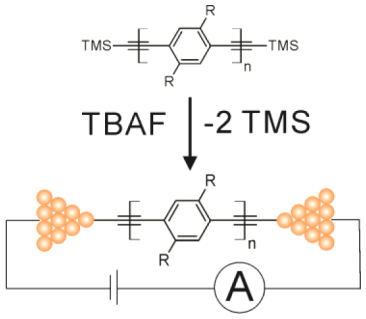

Scheme 2. Molecules Studied in This Work

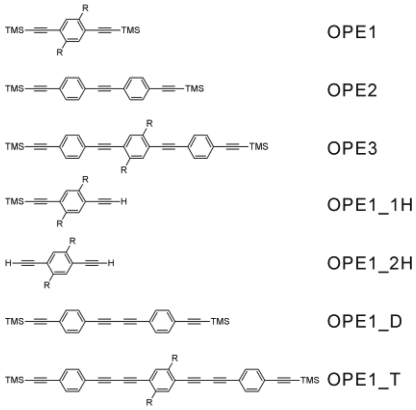

we demonstrate that a trimethylsilyl (TMS) group attached to an alkynyl moiety is cleaved in situ (i.e., in solution) in the presence of a base, such as tetrabutylammonium fluoride (TBAF), to create Au−C σ-bonds. As shown in Figure S2-1 (Supporting Information) [SI], deprotection with fluoride proceeds via formation of a pentavalent fluorosiliconate intermediate with loss of fluorotrimethylsilane to liberate an alkynylide as its tetrabutylammonium salt.[43−45] Clearly, the cleavage of the Si−C bond is through a heterolytic mechanism, similar to the cleavage of silyl ethers.[46] The generated alkynylide binds selectively to the adjacent gold surface, leading to the formation of a highly directional covalent Au−C σ−bond (Scheme 1).

We have synthesized a series of TMS-terminated oligo(phenylene ethynylene)s (OPEs) (Scheme 2, R = OCH_3) and measured single molecular conductances of these wires attached covalently to gold electrodes in solution by employing the mechanically controllable break junction (MCBJ) technique.[47] The transport measurements were combined with in situ STM imaging and gap-mode Raman spectroscopy to unravel the nature of surface binding. Importantly, this new concept to create Au−C σ-bonds paves the way toward further integration of functional molecules in molecular junctions employing easily accessible and versatile chemical strategies, thus providing a promising platform in nanoscale assembly.

EXPERIMENTAL SECTION

Chemicals and Organic Synthesis. Compounds OPE1,[48] OPE1_1H,[49] and OPE1_D[50] were synthesized according to literature procedures. Details of synthesis and characterization of OPE2, OPE3, and of the trimer OPE1_T are summarized in the Supporting Information (SI). All chemicals and solvents were purchased from commercial sources and used without further purification, unless specifically mentioned.

Conductance Measurements. The transport characteristics were studied in a mechanically controlled break junction setup (MCBJ). Single molecular junctions were created by the repeated opening and closing of a nanoscale gap between two gold electrodes, typically 500 ($t \leq 1000$ s) or 2000 ($t \geq 1000$ s) cycles with a stretching rate of 5 nm s^{-1} in a solution containing tetrahydrofuran (THF) | decane (v:v = 1:4), 0.5 mM of the TMS-protected target molecules and 1 mM TBAF. The conductance G (current/bias voltage) was measured as a function of the relative displacement Δz of the two electrodes. The individual traces were used to construct conductance histograms. Details of measurement technique and data analysis were reported in two previous studies of our group.[11,47] Specifics of the sample preparation with the TMS-protected OPE derivatives are described in SI.

Scanning Probe Experiments. The STM and AFM experiments were carried out on (111) facets of bead gold single crystals[51] mounted on a sheet of polycrystalline gold. Prior to each experiment, the electrode was subjected to electrochemical polishing and annealing in a hydrogen flame followed by cooling under Ar. Surface modification in the target molecule-containing solution was carried out in a sealed, stainless steel chamber in an argon atmosphere to avoid oxygen exposure. After a certain reaction time, the sample was removed from the assembly container, rinsed with THF, dried in argon, and subsequently inspected by STM or AFM.

The STM measurements were performed in decane using a Nanoscope E (Digital Instruments), which was equipped with a 1840AI scanner, in constant-current mode. The STM tips were prepared by mechanical cutting of Pt−Ir wires (80/20%, Pt/Ir, 0.25 mm in diameter, Goodfellow).

The AFM measurements were typically carried out in noncontact mode with a Nanosurf FlexAFM (Nanosurf AG, Switzerland) under ambient conditions and in air. We employed PPP-NCH-W cantilevers with a tip radius of ~10 nm (Nanosensors).

Raman Experiments. We employed gap-mode Raman spectroscopy[52−54] in Au(111) | target molecule | Au nanoparticle (NP) sandwich structures. The ~55 nm gold NPs were obtained using a modified citrate reduction method.[55] Details are summarized in the SI. The Au(111) substrates were prepared from 200-nm-thick gold films with a 5 nm chromium adhesion layer deposited on a glass wafer of 2 × 2 cm^2 size (Berliner Glas AG). The samples were cleaned in 98% concentrated sulfuric acid with extended rinsing with ultrapure water (Millipore, 3 ppb TOC), followed by flame annealing. Subsequently, the gold samples were immersed in the target solution, such as 0.5 mM OPE1 with 1 mM TBAF in THF. After a certain reaction time t, the gold films were taken out, rinsed with absolute ethanol (Aldrich, p.a.), dried in Ar (Carbagas, Alphagaz), and subsequently covered by drop-casting with a submonolayer (4−6 μL) of gold NPs.

Raman spectra of the dried samples were recorded with a HR 800 confocal Raman spectrometer (Horiba JY, France). The excitation wavelength was 632.8 nm from a He−Ne laser. A 50× magnification long-working-distance (8 mm) objective was used to focus the laser onto the sample and to collect the scattered light in a backscattering geometry. The power on the sample was about 1 mW.

RESULTS AND DISCUSSION

Figure 1A displays individual conductance traces from experiments with OPE1, OPE2, and OPE3 terminated at both ends with TMS groups. The data were recorded within the first 1000 s after adding TBAF to the sample-containing solution. We observe quantized charging conductance steps at integer multiples of the quantum conductance 1 G_0 upon elongation of the Au−Au junction until a single-atom contact between the two leads breaks at ~1 G_0. Subsequently, the conductance decreases abruptly to $G \leq 0.1$ G_0, depending on the molecular wire trapped, and well-defined single plateaus at molecule-dependent conductances appear. These features are attributed

dx.doi.org/10.1021/ja307544w | J. Am. Chem. Soc. 2012, 134, 19425−19431

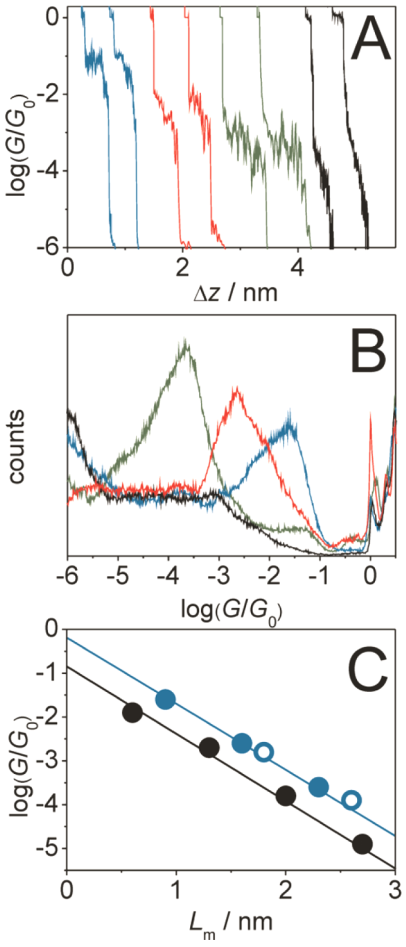

Figure 1. (A) Individual conductance-distance traces of OPE1 (blue), OPE2 (red), OPE3 (green), OPE1_1H (black) recorded in THF/decane (v:v = 1:4) + 1.0 mM TBAF and 0.5 mM target molecules, stretching rate ~5 nms^{-1}. (B) All-data point one-dimensional conductance histograms of OPE1, OPE2, OPE3, and OPE1_1H (Scheme 2) as constructed of 500 individual traces during the first 1000 s. (C) Most probable conductance of OPEs versus the molecular length L_m (filled blue circles, cf. Table S4–2 in SI). The black circles represent conductance data of the dithiol analogues taken from ref 58. Open blue circles indicate the most probable conductances of OPE1_D and OPE1_T.

to the conductance of (single) junctions formed between the deprotected targeted molecules covalently bound between the two gold point-contacts. The sample traces also show that the plateau length increases with molecular length and decreases upon stretching until junction rupture occurs with conductance values reaching the noise level. We note that the presence of electrolyte ions (TBA^+, F^-) determines the respective noise background level in our experiments at ~10^{-6} G_0.

Control experiments with asymmetric OPE1_1H wires having only one TMS-protecting group did not provide evidence for creation of molecular junctions. As an example, the black trace in Figure 1A displays an abrupt decrease of the conductance after breaking a single-atom gold contact at ~1 G_0 to approximately 10^{-3} G_0 followed by an exponential decay until the noise level is reached. This signature represents clearly a through-space tunneling behavior. The result further implies that TBAF as a nucleophilic catalyst and the applied electric field are not sufficient for cleaving the terminal C–H bond of the unprotected ethynyl group in OPE1_1H within a typical stretching cycle. The latter lasts about 100 ms. This observation is also supported by a high C–H bond dissociation energy of acetylene[56,57] as well as by the estimated pK_a(≡C–H) value of ~30.

Finally, we want to mention that no indications of molecular junction formation were observed in experiments with the blank solution containing only THF, decane, and 1 mM TBAF (see SI).

Typically, we recorded 2000 individual traces, which were subsequently analyzed by constructing all-data point histograms without any data selection to extract statistically significant results. Figure 1B displays the corresponding one-dimensional (1D) histogram in a logarithmic scale for three TMS-protected OPEs, together with data from the above control experiments. In addition to the Au–Au contact around 1 G_0, we found clear single peaks at $10^{-1.8}$ G_0, $10^{-2.7}$ G_0, and $10^{-3.6}$ G_0, which are assigned to the most probable molecular junction conductances before rupture of OPE1, OPE2, and OPE3, respectively. These values depend exponentially on the molecular length L_m according to $G \approx G_0 \exp(-\beta \cdot L_m)$ with a decay constant $\beta = (3.3 \pm 0.1)$ nm^{-1} (Figure 1C). This value is comparable with that of dithiol-terminated OPEs $\beta = (3.4 \pm 0.1)$ nm^{-1}, as obtained in our recent study under nearly identical experimental conditions.[58] We may conclude that the electron transfer across molecular junctions formed by deprotection of TMS-terminated OPEs proceeds by through-bond nonresonant tunneling. We also point out two additional distinct observations: (1) Extrapolation of the conductance data plotted in Figure 1C toward $L_m \rightarrow 0$ gives a value of approximately 1 G_0, indicating that the apparent contact resistance of the covalent bond formed is of the order of a metallic Au–Au nanocontact, thus indicating an excellent electronic coupling of the Au–C linker unit. (2) The comparison of these wires with their dithiol-terminated analogues reveals that the single molecular conductance values of the former are around one order of magnitude higher. The contact resistance per Au–S bond, ~40 kΩ, as obtained under experimental conditions the same as that for the Au–C data, is significantly larger.[58] Similar trends were reported in two recent studies by Venkataraman et al.,[27,28] which clearly indicates that our new approach based on TMS-deprotection chemistry represents a promising alternative to the $Sn(CH_3)_3$ route to form covalent, highly conductive Au–C contacts.

The above analysis was extended by constructing two-dimensional (2D) conductance vs displacement histograms.[19] This strategy provides direct access to the evolution of molecular junctions during the formation, elongation and breakdown steps (Figure 2A). We have introduced a relative displacement Δz with $\Delta z = 0$ at $G = 0.7$ G_0 to assign a common scale to each individual conductance vs distance trace. This procedure allows the accurate alignment of the conductance vs distance traces because of the sharp drop in conductance upon breaking the monatomic Au–Au contact at 1 G_0. Figure 2A displays the corresponding plot of OPE1 (for other data see SI). This graph shows a well-defined high-density data cloud with a clear conductance decay from 10^{-1} G_0 to $10^{-2.5}$ G_0 upon stretching up to $\Delta z \approx 0.35$ nm (region H, see SI for further details). This feature represents the stability range of a molecular junction. Extending the displacement to $\Delta z > 0.40$ nm leads to the breakdown of the molecular plateau region. The noise level is approached at $G < 10^{-5.5}$ G_0 (region T). The inset in Figure 2A displays the relative-displacement histograms[11] with a maximum at (0.35 ± 0.1) nm in the Δz scale as

dx.doi.org/10.1021/ja307544w | J. Am. Chem. Soc. 2012, 134, 19425–19431

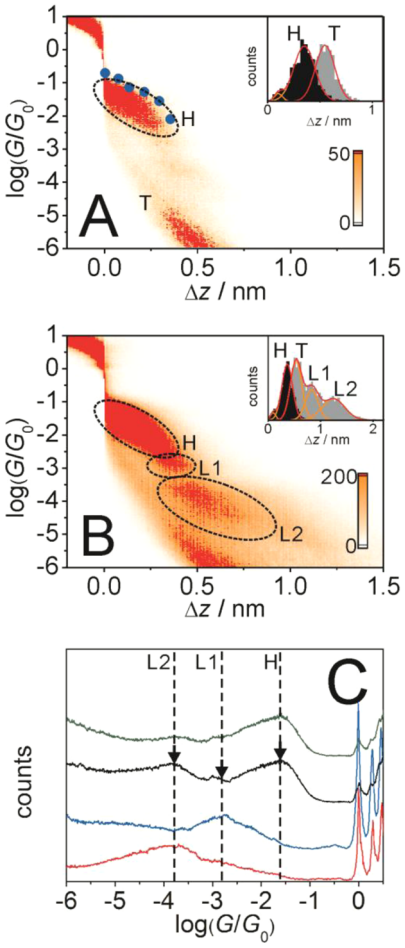

Figure 2. All-data point 2D conductance vs relative distance (Δz) histograms constructed from (A) 500 traces recorded during the first 1000 s and (B) long-term (3600 s) experiment with 2000 traces analyzed. The characteristic molecular conductance regions are labeled H, L1 and L2. The inset of (A) and (B) display relative-displacement histograms as obtained from an stretched distance analysis[47] in 0.7 G_0 to $10^{-2.5}$ G_0 (black) and up to 10^{-6} G_0 (gray). Panel (A) also shows the (scaled) conductance data (blue circles) from calculations reported in ref 42. (C) 1D conductance histograms of OPE1 recorded during the first 1000 s (green) and 3600 s (black) after the start of the experiment as well as of the dimer OPE1_D (blue) and of the trimer OPE1_T (red), both measured during the first 3600 s.

the most probably characteristic distance Δz^* over which a single OPE1 junction can be stretched. The narrow distribution of a single peak and the estimated junction formation probability of ~90% (calculated from the two peak area ratio in the inset of Figure 2A) demonstrate the uniformity and the high stability of the Au−C anchoring site. Considering the "snap-back" distance $\Delta z_{corr} \approx (0.50 \pm 0.1)$ nm[10,11,59] (see also SI), i.e. the fast relaxation of the electrode upon breaking a monatomic Au−Au contact, we obtain $z = \Delta z^* + \Delta z_{corr} = (0.85 \pm 0.20)$ nm as the most probable absolute electrode separation at which a single Au−OPE1−Au junction breaks. This value is comparable with the C−C distance 0.83 nm[42] of the two carbon atoms attached to the gold leads in a fully extended upright geometry.

In an attempt to qualitatively rationalize our experimental observations, we refer to recent electronic structure and transport calculations of ethynyl and diethynyl benzene attached to Au(111) leads.[39,42] By removal of the hydrogen of the ethynyl unit, the terminal carbon atom binds to the energetically most favorable three-fold hollow sites of two adjacent freshly broken gold leads. Other contact sites (bridge, atop) are also possible due to marginally small differences in the corresponding binding energies. At the immediate moment of breaking a monatomic Au−Au contact (Δz_{corr} = 0.5 nm) and cleaving the TMS protecting groups, the generated surface-bound intermediate is attached to the gold leads in a side[11] or tilted[42] geometry due to spatial restrictions. We hypothesize that a freshly broken Au−Au contact may bear a catalytic activity similar to that of a 'naked' Haruta-type Au nanocluster,[60,61] thus facilitating the cleavage of the TMS leaving group upon contact. Pulling the gold leads further apart causes an orientation change of the molecular wire in the gap from tilted toward more upright. The surface-bound species is quite mobile (barrier to surface diffusion on Au(111) ≈ 0.22 eV[39]), despite the strength of interaction with gold, and migrates from an fcc hollow toward an atop site, where the carbon atom is attached to a single gold atom.[39,42] The Au−C bond is stronger than the Au−Au bond and, as a consequence, the breaking of the molecular junction upon further stretching is accompanied by the detachment of a single gold atom from the surface, and not by the breaking of an Au−C bond. The latter represents a hybrid created by mixing the 2sp carbon orbital with the gold 5d orbitals, and thus provides a covalent carbon σ-bond to the gold surface.[39]

Hoft et al.[42] calculated transmission curves of relaxed Au−OPE1−Au molecular junctions at various stages of the pulling process, using a nonequilibrium Green's function technique. Their results are directly applicable to our experimental situation. These authors found a resonance feature at ~−1.0 eV, which tails into the Fermi level E_F at relatively high conductances (see also SI). The resonance is attributed to a 2sp(C)−5d(Au) σ-bonded hybrid, which mediates the electronic coupling at the interface.[39,42] The theoretically predicted high transmission through alkynyl−Au molecular junctions is also comparable with recent data reported for Au−C σ-bonded alkanes.[27] The transport calculations of Hoft et al.[42] predicted further that the broad transmission feature around E_F lowers upon stretching of a single molecular junction, which is attributed to a reduced coupling between the carbon and gold atoms as well as between the detached gold atoms and the rest of the surface.

Indeed, our experimental results support the theoretically predicted trends. Figure 2A displays, as an example, the comparison of the calculated conductances vs displacement data at various stages of the pulling process, as extracted from ref 42 (blue circles; for further details see transmission curves plotted in SI), with a set of real experimental data. The decrease in conductance with increasing displacement Δz is clearly resolved.

Despite the good agreement, we like to emphasize that the above comparison should be considered with caution and only treated as qualitative in nature. The DFT-based transport calculations in ref 42 did not account for self-energy errors and image charge corrections. However, as demonstrated previously by Cheng et al. in a study of Au−C σ-bonded alkanes, which are structurally related to our current system, these corrections downshift the σ-resonance toward slightly more negative energies (−0.90 eV) but do not change the qualitative trends.[27] This comparison supports and strengthens our interpretation.

The experimental data shown in Figure 1 and Figure 2A represent conductance vs displacement traces as recorded

dx.doi.org/10.1021/ja307544w | J. Am. Chem. Soc. 2012, 134, 19425−19431

during the first 1000 s after addition of THF/decane solution (v:v = 1:4) containing 0.5 mM TMS protected OPE1 and 1 mM TBAF into the liquid cell of the MCBJ setup. Extending the recording time to 3600 s and longer results in individual conductance traces with more than one plateau. The corresponding all-data point histograms either in a 1D (Figure 2C) or in a 2D (Figure 2B) representation show additional features. Figure 2B illustrates, as an example, the conductance vs relative displacement Δz for a series of 2000 OPE1 traces. In addition to the data cloud already assigned to the Au−C σ-bonded single molecular junctions of deprotected OPE1 monomers (region H), we observed two distinctly new conductance clouds around 10^{-3} G_0 and 10^{-4} G_0, which are labeled L1 and L2, respectively. Both features evolve more pronounced with progressing experimental time (see SI for details). Their relative-displacement (Δz) distribution, plotted as inset in Figure 2B, illustrates a representative distribution of the three characteristic conductance regions as obtained during 3600 s reaction time.

In an attempt to rationalize the nature of the evolving additional conductance features L1 and L2 we refer to recent reports on copper (Cu^+)- and gold (Au^+)-catalyzed oxidative coupling (dimerization) reactions of terminal alkynes.[62−66] These experiments lead to the corresponding symmetric 1,3-diynes in moderate to good yields and demonstrate the active role of a charged coinage metal in triggering the coupling reaction. On the basis of these results and considering that the application of a bias voltage between the two gold electrodes in the MCBJ configuration results in localized charges, we propose that the gold surface mediates the oxidative coupling to afford alkynylides. The mechanism is illustrated in SI, Figure S2-1. This interpretation is supported by NMR and Raman experiments of 0.5 mM OPE1 and 1 mM TBAF in THF solution, e.g. in the absence of a gold source. We observed no evidence of dimerization, even after 24 h of stirring.

On the basis of the above arguments and observations, we assign the new conductance features L1 and L2 to products of a slow oligomerization process. In an attempt to strengthen this hypothesis further, we synthesized the TMS-protected dimer and trimer of the OPE1 analogue, and measured these conductance characteristics within a time interval of 1000−3600 s (cf. Figure 2C and SI for details). The results of these experiments confirmed unambiguously that the additional features in the long-term reaction experiments of OPE1 represent conductances of the corresponding dimer OPE1_D (L1 region) and trimer OPE1_T (L2 region), respectively. This interpretation is also supported by the alignment of the latter conductance data (open blue circles in Figure 1C) with the linear relation log (G/G_0) vs molecular length L_m (filled circles in Figure 1C).

Similar results are also predicted for the other two OPE derivatives. However, the expected single-junction conductance data of the corresponding dimers and trimers were not observed. This may be related to the reduced reactivity of the longer wires or to the fact that the conductances of the corresponding dimers and trimers are below the detection limit of our current setup. In concluding this paragraph we emphasize that a careful choice of experimental conditions provides a sufficiently large time interval, within which single molecular junctions of the Au−C σ-bonded monomers could be identified and characterized without interference of coexisting oligomers.

Next we present results of structure-sensitive experiments, specifically STM imaging and gap-mode Raman spectroscopy,[52−54] which provide evidence for the formation of surface-confined covalent Au−C≡C−R bonds under conditions similar to those applied in the MCBJ measurements. STM experiments revealed a major restructuring of a freshly prepared Au(111) (1 × 1) surface in THF containing 1 mM TBAF upon addition of 0.5 mM OPE1 (Figure 3). Within less than 1000 s

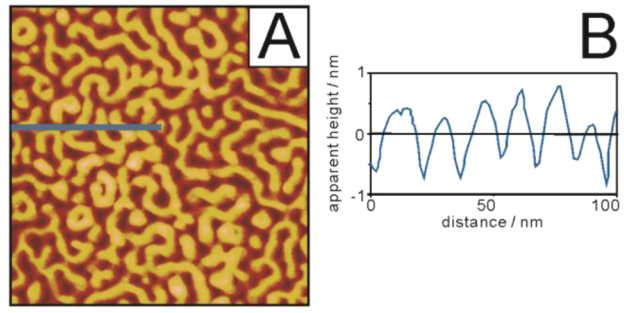

Figure 3. (A) STM image recorded in decane, size 200 nm × 200 nm and (B) typical cross section of an Au(111) surface after 1000 s exposure to a 0.5 mM OPE1/1.0 mM TBAF solution in THF (for further details see SI) and cross-section analysis of the blue line.

monatomically deep vacancy islands and channels as well as terraces develop as a result of the restructuring of the gold surface over up to five atomic layers. Control experiments with THF/decane + 1 mM TBAF and THF/decane + 0.5 mM OPE1 showed clearly that the observed structure changes are not related to the known gentle etching of a Au(111) surface in THF (see also SI for details)[67] but rather represent the result of a surface-confined chemical reaction. We speculate that this reaction comprises the formation of a covalent Au−C bond through the alkynylide, which is generated by the fluoride-induced cleavage of the TMS-leaving group, most probably in direct contact with the gold surface. The comparison of our results with a recent STM report on grafting ethynylbenzene on Au(111)[40] demonstrates convincingly that the formation of covalent Au−C σ-bonds using TMS-protected precursors proceeds more efficiently, and even at room temperature, indicating that H-terminated ethynyl groups require additional energy due to the endothermic breaking of the C−H σ-bond.[39,40]

Additional evidence for the formation of covalent Au−C σ-bonds is obtained from gap-mode Raman spectroscopic experiments. We created Au molecule | (OPE1, OPE2, or OPE3) | Au nanoparticle (NP) sandwich structures (Figure 4). The adlayer was obtained by surface grafting from a THF/decane solution containing 1 mM TBAF and 0.5 mM of the target molecule, under argon to avoid the presence of oxygen. The reaction was stopped at various time intervals. After extended rinsing of the modified gold surface with ethanol to remove unbound material, a submonolayer of citrate-stabilized gold NPs was deposited to create nanoplasmonic gaps. Figure 4 displays Raman spectra of OPE1 as observed for 1000 and 3600 s reaction time during the immobilization process. The graphs in Figure 4 show clear Raman signals at 1297 cm^{-1} (δ_{CH}), 1593 cm^{-1} (ν_{Ring}), 1900−2200 cm^{-1} ($\nu_{C\equiv C}$), and between 2800 to 3100 (ν_{C-H}), which confirm the surface immobilization of OPE1. Details of the band assignment, as well as additional Raman and SERS spectra of the various compounds, which

dx.doi.org/10.1021/ja307544w | J. Am. Chem. Soc. 2012, 134, 19425−19431

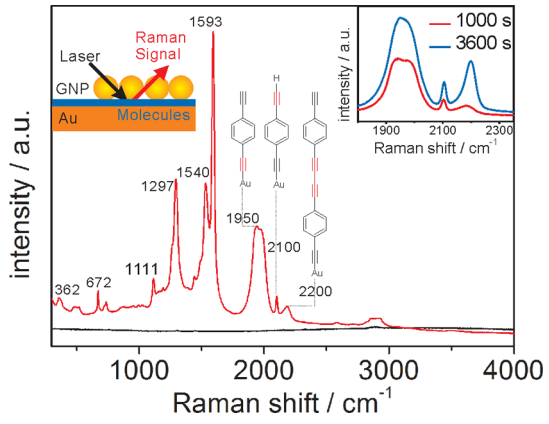

Figure 4. Gap-mode Raman spectra of a gold surface immersed in THF solution containing 0.5 mM OPE1 with (red line) and without (black line) TBAF for 1000 s. The left panel illustrates the schematics of the gap-mode configuration. The right panel represents a magnification of the spectra in the C≡C stretching region recorded after 1000 s (red) and after 3600 s (blue) reaction time.

were investigated under a wide range of different experimental conditions, are summarized in the SI.

In this paragraph we discuss data of OPE1 as recorded during the first 1000 s of surface modification. The $\nu_{C\equiv C}$ stretching region in the SERS spectra is particularly informative. The single stretching mode as monitored in the normal Raman spectra at ~2150 cm^{-1}, due to the free C≡C group, is found to broaden and to downshift to 1950 cm^{-1}. The red-shift of ~200 cm^{-1} indicates that the OPE1 molecules are bound to the gold substrate. Both observations indicate a strong interaction with the substrate. This result is in agreement with previous reports on the formation of covalent Au−C bonds involving −C≡C− linkers.[37,38,41] The appearance of a small band at ~2100 cm^{-1}, which represents the spectral position of a free C≡C group, provides evidence that the deprotected OPE is adsorbed on a planar Au(111) surface mainly through one of the two acetylene groups with the other being pendent and/or only weakly (electrostatically) attached to adjacent Au-NPs in the top layer.[37,38] A remarkable change in the Raman spectra is found for samples exposed 3600 s or longer to the assembly solution (inset in Figure 4). In addition to the two ν(C≡C) bands already described, we detected a third band around 2200 cm^{-1}. Comparative Raman experiments with OPE2 and OPE3 in normal Raman and upon immobilization on Au(111) demonstrated that this spectral feature represents (C≡C) groups interspaced between adjacent phenyl rings of the molecular rod (see SI for details). These results demonstrate that the appearance of these bands provides direct evidence of forming surface-confined oligomers in long-time assembly/reaction experiments with OPE1. Thus, the interpretation of our transport experiments is nicely supported. We also notice that the application of a negative charge to the gold leads quenches dimerization, whereas the Au−C covalent bond formation is selectively preserved. Paragraph 6.6 in SI summarizes SERS experiments at the electrochemical gold/electrolyte interface, which support this important discovery on selectivity.

CONCLUSION

To conclude, we have developed a new and efficient approach to create covalent Au−C anchoring sites based on TMS-protecting group chemistry. Employing the MCBJ technique in liquid, we demonstrated the formation of highly conducting single molecular junctions of several OPE-derivatives attached to Au leads. However, we also demonstrated that extended assembly and reaction times lead to oligomerization. The created junctions are mechanically stable and exhibit conductances around one order of magnitude higher as compared to those of traditional anchoring groups. Binding geometry and junction evolution were discussed by comparing our experimental observations with theoretical predictions. The latter could be confirmed convincingly. Structure evidence to support the formation of covalent Au−C σ-bonds is derived from STM imaging and gap-mode Raman experiments. On the basis of the combination of structure and transport measurements we could identify experimental conditions under which selectively only monomeric Au−OPE−Au junctions were created. Anchoring (functional) molecular wires through alkynyl groups covalently attached to contact leads could benefit from the rich chemistry available and offers considerable promise in the further development of fundamental and applied single-molecule charge transport studies. Use-inspired basic research will lead us to further apply this new strategy to a variety of π-conjugated systems with specific functions in a straightforward manner thanks to the broad variability of the TMS-protected molecules.

ASSOCIATED CONTENT

Supporting Information

Details on the molecular synthesis, the experimental setup, data analysis, and the Raman and SPM measurements. This material is available free of charge via the Internet at http://pubs.acs.org.

AUTHOR INFORMATION

Corresponding Author

liu@iac.unibe.ch (S.-X.L.); thomas.wandlowski@dcb.unibe.ch (T.W.)

Notes

The authors declare no competing financial interest.

ACKNOWLEDGMENTS

We acknowledge particularly the enlightening discussions with P. Renaud on the mechanism of the TMS-cleaving reaction. This work was also supported by the Swiss National Science Foundation (Grant Nos. 200020-116003, 200020-144471, and 200021-124643) and by EC FP7 ITN "FUNMOLS", Project 212942.

REFERENCES

(1) Cuevas, J. C.; Scheer, E. *Molecular Electronics: An Introduction to Theory and Experiment*; World Scientific Series in Nanoscience and Nanotechnology; World Scientific: Singapore, 2010.
(2) Chen, F.; Hihath, J.; Huang, Z. F.; Li, X. L.; Tao, N. J. *Annu. Rev. Phys. Chem.* **2007**, *58*, 535−564.
(3) McCreery, R. L.; Bergren, A. J. *Adv. Mater. (Weinheim, Ger.)* **2009**, *21*, 4303−4322.
(4) Metzger, R. M. *Unimolecular and Supramolecular Electronics II*; Topics in Current Chemistry *313*; Springer Verlag: Berlin, 2012.
(5) Kiguchi, M.; Kaneko, S. *ChemPhysChem* **2012**, *13*, 1116−1126.
(6) Chen, F.; Li, X.; Hihath, J.; Huang, Z.; Tao, N. *J. Am. Chem. Soc.* **2006**, *128*, 15874−15881.
(7) Li, C.; Pobelov, I.; Wandlowski, T.; Bagrets, A.; Arnold, A.; Evers, F. *J. Am. Chem. Soc.* **2008**, *130*, 318−326.
(8) Hybertsen, M. S.; Venkataraman, L.; Klare, J. E.; Cwhalley, A.; Steigerwald, M. L.; Nuckolls, C. *J. Phys.: Cond. Matt.* **2008**, *20*, 374115.
(9) Xu, B. Q.; Tao, N. J. J. *Science* **2003**, *301*, 1221−1223.

(10) Quek, S. Y.; Kamenetska, M.; Steigerwald, M. L.; Choi, H. J.; Louie, S. G.; Hybertsen, M. S.; Neaton, J. B.; Venkataraman, L. *Nat. Nanotechnol.* **2009**, *4*, 230−234.
(11) Hong, W.; Manrique, D. Z.; Moreno−Garcia, P.; Gulcur, M.; Mishchenko, A.; Lambert, C. J.; Bryce, M. R.; Wandlowski, T. *J. Am. Chem. Soc.* **2012**, *134*, 2292−2304.
(12) Venkataraman, L.; Klare, J. E.; Tam, I. W.; Nuckolls, C.; Hybertsen, M. S.; Steigerwald, M. L. *Nano Lett.* **2006**, *6*, 458−462.
(13) Kim, B.; Beebe, J. M.; Jun, Y.; Zhu, X. Y.; Frisbie, C. D. *J. Am. Chem. Soc.* **2006**, *128*, 4970−4971.
(14) Mishchenko, A.; Zotti, L. A.; Vonlanthen, D.; Burkle, M.; Pauly, F.; Cuevas, J. C.; Mayor, M.; Wandlowski, T. *J. Am. Chem. Soc.* **2011**, *133*, 184−187.
(15) Zotti, L. A.; Kirchner, T.; Cuevas, J. C.; Pauly, F.; Huhn, T.; Scheer, E.; Erbe, A. *Small* **2010**, *6*, 1529−1535.
(16) Ko, C. H.; Huang, M. J.; Fu, M. D.; Chen, C. H. *J. Am. Chem. Soc.* **2010**, *132*, 756−764.
(17) Park, Y. S.; Whalley, A. C.; Kamenetska, M.; Steigerwald, M. L.; Hybertsen, M. S.; Nuckolls, C.; Venkataraman, L. *J. Am. Chem. Soc.* **2007**, *129*, 15768−15769.
(18) Xing, Y.; Park, T.−H.; Venkatramani, R.; Keinan, S.; Beratan, D. N.; Therien, M. J.; Borguet, E. *J. Am. Chem. Soc.* **2010**, *132*, 7946−7956.
(19) Martin, C. A.; Ding, D.; Sorensen, J. K.; Bjornholm, T.; van Ruitenbeek, J. M.; van der Zant, H. S. J. *J. Am. Chem. Soc.* **2008**, *130*, 13198−13199.
(20) Kiguchi, M. *Appl. Phys. Lett.* **2009**, *95*, 073301.
(21) Fock, J.; Sorensen, J. K.; Loertscher, E.; Vosch, T.; Martin, C. A.; Riel, H.; Kilsa, K.; Bjornholm, T.; van der Zant, H. *Phys. Chem. Chem. Phys.* **2011**, *13*, 14325−14332.
(22) Leary, E.; Teresa Gonzalez, M.; van der Pol, C.; Bryce, M. R.; Filippone, S.; Martin, N.; Rubio−Bollinger, G.; Agrait, N. *Nano Lett.* **2011**, *11*, 2236−2241.
(23) Kristensen, I. S.; Mowbray, D. J.; Thygesen, K. S.; Jacobsen, K. W. *J. Phys.: Condens. Matter* **2008**, *20*, 374101.
(24) Arroyo, C. R.; Leary, E.; Castellanos−Gomez, A.; Rubio−Bollinger, G.; Teresa Gonzalez, M.; Agrait, N. *J. Am. Chem. Soc.* **2011**, *133*, 14313−14319.
(25) Kiguchi, M.; Tal, O.; Wohlthat, S.; Pauly, F.; Krieger, M.; Djukic, D.; Cuevas, J. C.; van Ruitenbeek, J. M. *Phys. Rev. Lett.* **2008**, *101*, 046801.
(26) Schneebeli, S. T.; Kamenetska, M.; Cheng, Z.; Skouta, R.; Friesner, R. A.; Venkataraman, L.; Breslow, R. *J. Am. Chem. Soc.* **2011**, *133*, 2136−2139.
(27) Cheng, Z. L.; Skouta, R.; Vazquez, H.; Widawsky, J. R.; Schneebeli, S.; Chen, W.; Hybertsen, M. S.; Breslow, R.; Venkataraman, L. *Nat. Nanotechnol.* **2011**, *6*, 353−357.
(28) Chen, W.; Widawsky, J. R.; Vazquez, H.; Schneebeli, S. T.; Hybertsen, M. S.; Breslow, R.; Venkataraman, L. *J. Am. Chem. Soc.* **2011**, *133*, 17160−17163.
(29) Delamar, M.; Hitmi, R.; Pinson, J.; Saveant, J. M. *J. Am. Chem. Soc.* **1992**, *114*, 5883−5884.
(30) Dyke, C. A.; Tour, J. M. *J. Am. Chem. Soc.* **2003**, *125*, 1156−1157.
(31) Gooding, J. J.; Ciampi, S. *Chem. Soc. Rev.* **2011**, *40*, 2704−2718.
(32) Ricci, A. M.; Calvo, E. J.; Martin, S.; Nichols, R. J. *J. Am. Chem. Soc.* **2010**, *132*, 2494−2495.
(33) Chehmiledl, M. M. *Aryl Diazonium Salts*; Wiley: New York, 2012.
(34) Long, N. J.; Williams, C. K. *Angew. Chem., Int. Ed.* **2003**, *42*, 2586−2617.
(35) Schuster, O.; Liau, R. Y.; Schier, A.; Schmidbaur, H. *Inorg. Chim. Acta* **2005**, *358*, 1429−1441.
(36) Feilchenfeld, H.; Weaver, M. J. *J. Phys. Chem.* **1989**, *93*, 4276−4282.
(37) Joo, S.−W.; Kim, K. *J. Raman Spectrosc.* **2004**, *35*, 549−554.
(38) Lim, J. K.; Joo, S.-W.; Shin, K. S. *Vib. Spectrosc.* **2007**, *43*, 330−334.
(39) Ford, M. J.; Hoft, R. C.; McDonagh, A. *J. Phys. Chem. B* **2005**, *109*, 20387−20392.
(40) McDonagh, A. M.; Zareie, H. M.; Ford, M. J.; Barton, C. S.; Ginic-Markovic, M.; Matisons, J. G. *J. Am. Chem. Soc.* **2007**, *129*, 3533−3538.
(41) Maity, P.; Wakabayashi, T.; Ichikuni, N.; Tsunoyama, H.; Xie, S.; Yamauchi, M.; Tsukuda, T. *Chem. Commun.* **2012**, *48*, 6085−6087.
(42) Hoft, R. C.; Ford, M. J.; Garcia−Suarez, V. M.; Lambert, C. J. *J. Phys.: Condens. Matter* **2008**, *20*, 025207.
(43) Schelhaas, M.; Waldmann, H. *Angew. Chem., Int. Ed.* **1996**, *35*, 2056−2083.
(44) Sieber, P. *Helv. Chim. Acta* **1977**, *60*, 2711−2716.
(45) Ernst, A.; Gobbi, L.; Vasella, A. *Tetrahedron Lett.* **1996**, *37*, 7959−7962.
(46) Kocieński, P. J. *Protecting Groups*, 3rd ed.; Georg Thieme Verlag; Stuttgart, 2005.
(47) Hong, W.; Valkenier, H.; Mészáros, G.; Manrique, D. Z.; Mishchenko, A.; Putz, A.; García, P. M.; Lambert, C. J.; Hummelen, J. C.; Wandlowski, T. *Beilstein J. Nanotechnol.* **2011**, *2*, 699−713.
(48) Yi, C.; Blum, C.; Lehmann, M.; Keller, S.; Liu, S.-X.; Frei, G.; Neels, A.; Hauser, J.; Schürch, S.; Decurtins, S. *J. Org. Chem.* **2010**, *75*, 3350−3357.
(49) Rodriguez, J. G.; Tejedor, J. L.; La Parra, T.; Diaz, C. *Tetrahedron* **2006**, *62*, 3355−3361.
(50) Draper, S. M.; Delamesiere, M.; Champeil, E.; Twamley, B.; Byrne, J. J.; Long, C. *J. Organomet. Chem.* **1999**, *589*, 157−167.
(51) Clavilier, J.; Armand, D.; Sun, S. G.; Petit, M. *J. Electroanal. Chem.* **1986**, *205*, 267−277.
(52) Ikeda, K.; Fujimoto, N.; Uehara, H.; Uosaki, K. *Chem. Phys. Lett.* **2008**, *460*, 205−208.
(53) Li, J. F.; Huang, Y. F.; Ding, Y.; Yang, Z. L.; Li, S. B.; Zhou, X. S.; Fan, F. R.; Zhang, W.; Zhou, Z. Y.; Wu, D. Y.; Ren, B.; Wang, Z. L.; Tian, Z. Q. *Nature* **2010**, *464*, 392−395.
(54) Cui, L.; Liu, B.; Vonlanthen, D.; Mayor, M.; Fu, Y.; Li, J.−F.; Wandlowski, T. *J. Am. Chem. Soc.* **2011**, *133*, 7332−7335.
(55) Frens, G. *Nature Phys. Sci.* **1973**, *241*, 20−22.
(56) Shiromaru, H.; Achiba, Y.; Kimura, K.; Lee, Y. T. *J. Phys. Chem.* **1987**, *91*, 17−19.
(57) Segall, J.; Lavi, R.; Wen, Y.; Wittig, C. *J. Phys. Chem.* **1989**, *93*, 7287−7289.
(58) Kaliginedi, V.; Moreno-Garcia, P.; Valkenier, H.; Hong, W.; Garcia-Suarez, V. M.; Buiter, P.; Otten, J. L. H.; Hummelen, J. C.; Lambert, C. J.; Wandlowski, T. *J. Am. Chem. Soc.* **2012**, *134*, 5262−5275.
(59) Agrait, N.; Yeyati, A. L.; van Ruitenbeek, J. M. *Phys. Rep.* **2003**, *377*, 81−279.
(60) Haruta, M. *Chem. Rec. (New York, NY)* **2003**, *3*, 75−87.
(61) Haruta, M.; Date, M. *Appl. Catal., A* **2001**, *222*, 427−437.
(62) Kamata, K.; Yamaguchi, S.; Kotani, M.; Yamaguchi, K.; Mizuno, N. *Angew. Chem., Int. Ed.* **2008**, *47*, 2407−2410.
(63) Adimurthy, S.; Malakar, C. C.; Beifuss, U. *J. Org. Chem.* **2009**, *74*, 5648−5651.
(64) Yin, W.; He, C.; Chen, M.; Zhang, H.; Lei, A. *Org. Lett.* **2009**, *11*, 709−712.
(65) Chen, Z.; Jiang, H.; Wang, A.; Yang, S. *J. Org. Chem.* **2010**, *75*, 6700−6703.
(66) Zhu, M.; Ning, M.; Fu, W.; Xu, C.; Zou, G. *Bull. Korean Chem. Soc.* **2012**, *33*, 1325−1328.
(67) Barden, W. R. T.; Singh, S.; Kruse, P. *Langmuir* **2008**, *24*, 2452−2458.